THERMAL MEASUREMENTS USING LASER FLASH ANALYSIS AND FREQUENCY-DOMAIN THERMOREFLECTANCE

A Thesis

Presented to the Faculty of the Graduate School

Of Cornell University

In Partial Fulfillment of the Requirements for the degree of Master of Science

By

Zhi Wang

August 2021

ABSTRACT

Thermal measurement is a critical part of determining the thermal properties of materials. Conventional steady-state thermal conductivity measurements have strict requirements on the sample dimensions and states, making it hard to measure most unconventional samples. Laser flash analysis (LFA) is a convenient and reliable method of determining different materials' thermal diffusivity and thermal conductivity. Apart from LFA, FDTR (Frequency Domain Thermoreflectance) is a much more powerful tool for thermal measurements, where samples with almost all dimensions and states can be measured. FDTR is thermal property microscopy that utilizes two lasers (pump and probe lasers) to measure the samples' thermal properties. The periodically modulated pump laser locally heats the sample. The probe laser detects the surface reflectivity of the sample, which can be used to calculate the thermal properties of the sample with models. Instead of only measuring the sample's thermal conductivity, the FDTR system can measure up to two properties at once – including volumetric heat capacity, thermal conductivity, thickness, interfacial conductivity, and the anisotropic ratio of thermal conductivity of the sample.

This thesis demonstrates how LFA works and how it conducts measurements for polymeric composites and polymer blend samples. Also, this thesis concludes on how to set up an FDTR system and how it works on thermal measurements.

BIOGRAPHICAL SKETCH

Zhi Wang was born on October 9, 1996, in Ningbo, Zhejiang Province, to Hongbo Wang and Wei Wang. He attended BUCT (Beijing University of Chemical Technology) with a major in Polymer Engineering from 2015 to 2019. He conducted his research in the Research Center of the Ministry of Education for High Gravity Engineering and Technology, a national key laboratory in Beijing. After graduation with a bachelor's degree, Zhi was admitted to Cornell University in material science. He hence moved to Ithaca, NY, and joined Prof. Zhiting Tian's group at the MAE department. During graduate study and research, his main focus is on thermal measurement techniques and thermal conducting materials.

For mom, dad, and friends

ACKNOWLEDGEMENTS

First, I want to give my most sincere gratitude to my committee members and professors who taught, inspired and helped me during my master's journey at Cornell. I want to thank my principal investigator and mentor, Professor Zhiting Tian, who welcomed me into her group with her enthusiasm in research and kindness in helping me adjusting myself for graduate study. Also, I should thank Professor Meredith Silberstein for her kindness and help. Apart from my committee members, I want to thank Professor Kit Umbach, who taught me lectures with his profound knowledge and helped me through my graduate school applications. In addition, I want to give my appreciation to Professor Richard D. Robinson, Professor Pete Bocko, and Professor Andrej Singer for their help during my graduate study.

Second, I want to thank those who helped my conducting my research work at Cornell. I want to thank Dr. Hao Ma, Dr. Jiefu Yin for teaching me to learn and do research on FDTR and LFA. Also, I should thank Renjiu Hu, Chen Li for helping me with my research.

Finally, I want to thank all my friends and family members for supporting and help me during my graduate study. I want to thank my sister Shanni and other friends for supporting me through the most challenging time during this challenging year under pandemic.

Thank you.

TABLE OF CONTENT

LIST OF FIGURES

1. Introduction to thermal measurements

Thermal conductivity is a fundamental property of a material to conduct heat under a temperature difference, which delineates how well a material conducts heat. It is a property essential in fabricating advanced materials and systems. As more and more new materials and material systems keep emerging, they pose new challenges for measuring techniques[1] – more complex sample requirements and measurement accuracy requirements. Only faster and more sophisticated thermal measurement tools can deal with modern microelectronics and high-level material systems.[2]

There are three different thermal measurements – steady-state method[3], frequency-domain transient methods[4], and time-domain transient methods[5]. For steady-state measurement, it accomplishes its measurements by reaching a steady-state temperature gradient, where the temperature of any part does not change with time.[3] This method is the most fundamental technique of measuring thermal conductivities, and it is directly based on Fourier's law of heat transfer. However, this method suffers from low accuracy and slow measurement speed. Moreover, this method also has strict requirements on what kind of samples it can measure[6]. The other two methods are transient methods, where the temperature does not persist at any place on the sample. The temperature is either dependent on the frequency (frequency-domain) or the time (time-domain). In this thesis, LFA is given as an example of a time-domain transient method, and FDTR is given as an example of a frequency-domain transient method. These two methods overcame the shortcomings of steady-state methods and opened opportunities for measuring much more complex samples.

References

[1] Regner, K. T. *et al.* Broadband phonon mean free path contributions to thermal conductivity measured using frequency domain thermoreflectance. *Nat. Commun.* **4**, 1640–1647 (2013).

[2] Zhao, W., Yang, Y., Bao, Z., Yan, D. & Zhu, Z. Methods for measuring the effective thermal conductivity of metal hydride beds: A review. *Int. J. Hydrogen Energy* **45**, 6680–6700 (2020).

[3] Hapenciuc, C. L., Negut, I., Borca-Tasciuc, T. & Mihailescu, I. N. A steady-state hot-wire method for thermal conductivity measurements of fluids. *Int. J. Heat Mass Transf.* **134**, 993–1002 (2019).

[4] Tang, L. & Dames, C. Anisotropic thermal conductivity tensor measurements using beam-offset frequency domain thermoreflectance (BO-FDTR) for materials lacking in-plane symmetry. *Int. J. Heat Mass Transf.* **164**, 120600 (2021).

[5] Yue, S. *et al.* Photoluminescence mapping and time-domain thermo-photoluminescence for rapid imaging and measurement of thermal conductivity of boron arsenide. *Mater. Today Phys.* **13**, (2020).

[6] Matrose, N. A., Obikese, K., Belay, Z. A. & Caleb, O. J. Thermal conductivity of insulating refractory materials: comparison of steady-state and transient measurement methods Diana. *Sci. Total Environ.* 135907 (2019). doi: 10.1016/j.oceram.2021.100118

2. Steady-state thermal conductivity measurement method

As the most basic measurement for thermal conductivity, Steady-state is a technique measuring the sample's thermal conductivity when its temperature distribution does not change in the timeframe of measurements. Based on Fourier's law of heat transfer, we have the mechanism for the steady-state method, [1]

$$k = \frac{QL}{A\Delta T} \tag{1}$$

Where Q is the heat flow through the sample, A is the cross-section area of the sample where heat flows through, L is the distance between temperature sensors and ΔT is the temperature difference between these sensors.

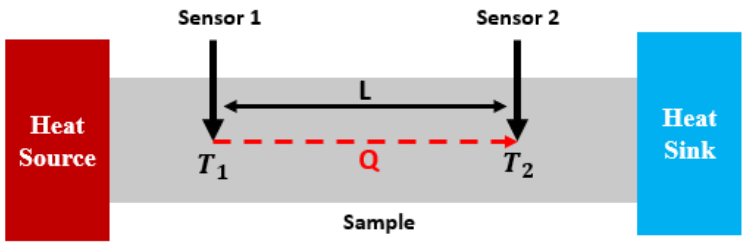

Figure 1: Schematic of Steady-State thermal measurement method

Typical steady-state measurement equipment consists of a heat sink, heat source, two sensors, and a heat flow detector. For measurements, this equipment will need a well-machined sample with a known cross-section area. Two thermometers give the real-time temperature of the temperature at the measuring point. For measurement, the heat source will heat the sample and take the temperature of the two sensors after the heat flow in the sample reaches a steady-state (temperature does not change with time for both sensors). Then, with heat flow reading from the detector, apply Fourier's law of heat conduction, thermal conductivity can be calculated.[2-4]

This method has strict requirements on the samples[3], where the samples must be bulk and machined to the measuring chamber's size. Also, thermal damage can happen during measurement if the sample is heat sensitive. Furthermore, the accuracy of this method is very low, which can be attributed to parasitic heat losses, contact thermal resistance from the sensors and radiation heat loss. Overall, this method is inefficient in measuring speed (long waiting time for steady-state) and measurement accuracy.[5]

References

[1] Zhao, D., Qian, X., Gu, X., Jajja, S. A. & Yang, R. Measurement techniques for thermal conductivity and interfacial thermal conductance of bulk and thin film materials. *J. Electron. Packag. Trans. ASME* **138**, 1–19 (2016).

[2] Kraemer, D. & Chen, G. A simple differential steady-state method to measure the thermal conductivity of solid bulk materials with high accuracy. *Rev. Sci. Instrum.* **85**, (2014).

[3] Roder, H. M., Perkins, R. A., Laesecke, A. & Nieto De Castro, C. A. Absolute steady-state thermal conductivity measurements by use of a transient hot-wire system. *J. Res. Natl. Inst. Stand. Technol.* **105**, 221–253 (2000).

[4] J.L.Nagy, L. L. Investigation of the steady state measurement process. *J. Automat. Chem.* **10**, 101–105 (1988).

[5] Slifka, A. J. Thermal-Conductivity Apparatus for Steady-State, Comparative Measurement of Ceramic Coatings. *J. Res. Natl. Inst. Stand. Technol.* **105**, 591–605 (2000).

3. Laser flash introduction (time-domain transient method)

Unlike steady-state measurement, the time-domain transient method measures the sample heating process. The heat sources are usually pulsed or periodically supplied for the transient method, leading to transient and periodic temperature changes in the material. These changes will lead to phase signal and amplitude signal output, respectively.[1]

Compared to thermal conductivity, thermal diffusivity is much easier to measure, and the accuracy is also higher. Thermal diffusivity describes the heat flow rate through the material, which is directly related to thermal conductivity. Laser flash is one kind of transient time-domain method that accurately and rapidly gives thermal diffusivity measurements.[2] Moreover, thermal conductivity can be calculated from the thermal diffusivity measurements when combined with other parameters.[3]

The thermal diffusivity of all samples is measured with the laser flash method, which is applied by assuming that the samples are all homogeneous. Thermal conductivity is calculated with this equation with the as-measured thermal diffusivity.[4]

$$k(T) = C_P(T) * \rho(T) * \alpha(T) \quad (2)$$

Where k is thermal conductivity, C_P is heat capacity from DSC measurements, ρ is the bulk density and α is the thermal diffusivity determined by laser flash method.

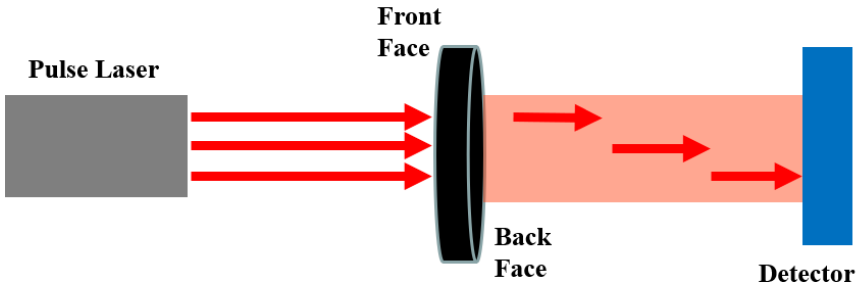

Figure 2: Schematic of LFA mechanism

LFA works on the assumption that there is a temperature response on the back of the sample after pulsed laser heating. This assumption should adhere to the following equations[5-7]

$$\Delta T = \Delta T_m[1 + 2\sum_{n=1}^{\infty}(-1)^n \exp\left(\frac{-n^2\pi^2\alpha t}{L^2}\right)] \quad (3)$$

Where L is the thickness of the sample, α is thermal diffusivity, ΔT is the temperature change in the sample, ΔT_m is the maximum value, t stands for the time passed after the pulse.

$t_{\frac{1}{2}}$ is defined as when the temperature rises to

$$\frac{\Delta T}{\Delta T_m} = \frac{1}{2} \quad (4)$$

And thermal diffusivity can be calculated with the equation

$$\alpha = \frac{0.1388L^2}{t_{\frac{1}{2}}} \quad (5)$$

However, more advanced fitting can yield much more accurate results than this method, and in this thesis, a combined model is used for fitting thermal diffusivity.

3.1 XFALT System

Linseis XFA 500 Xenon Flash Thermal Constant Analyzer (XFALT) was used for thermal diffusivity measurements. XFALT employs a high-energy laser beam as the heating source, where the laser pulse gets fully absorbed by the sample. For best absorption of laser energy and emission for an infrared thermal response, both sides of the sample were coated with a thin layer of graphite to optimize the signal-to-noise ratio. The change in emission was subsequently detected and analyzed by a high-speed liquid nitrogen-cooled IR sensor. A combined model that included heat loss and finite pulse correction gave thermal diffusivity of the samples. For measurement, samples were pre-cut into 1-inch pellets for the standard silicon carbide sample holder, and the furnace under the laser flash was set to 20 °C in 1 atm to balance

the temperature of the samples. Each sample was measured more than five times (deviation <5%), and the average value of thermal diffusivity was used.

3.2 Thermal diffusivity measurements for BN/silicone composites

3.2.1 BN/silicone sample preparation

Two-part self-curing silicone rubber is purchased from TAP plastic company, where the TAP Platinum Silicone system comprises two parts (side A as vinyl-terminated silicone base and side B hydride-terminated part with platinum-containing catalyst). Micron-sized BN powder is purchased from VWR international.

Tap platinum silicone has a very high molecular weight. In order to lower the viscosity, an equal amount (volume) of toluene is used to dilute the silicone rubber oligomers. After dilution of silicone rubber, BN powder is added to the solution. Then, the blender undergoes vigorous mechanical stirring for 2 h. The solution is then poured into a mold coated with a demolding agent. A smooth and homogenous silicone/BN composite can be obtained after the evaporation of toluene and the curing of two parts. A series solid content (0 wt%, 5 wt%, 10 wt%, 15 wt%, 20 wt%, and 30 wt%) of silicone/BN composites are obtained from this method.

3.2.2 Measurements for BN/silicone sample

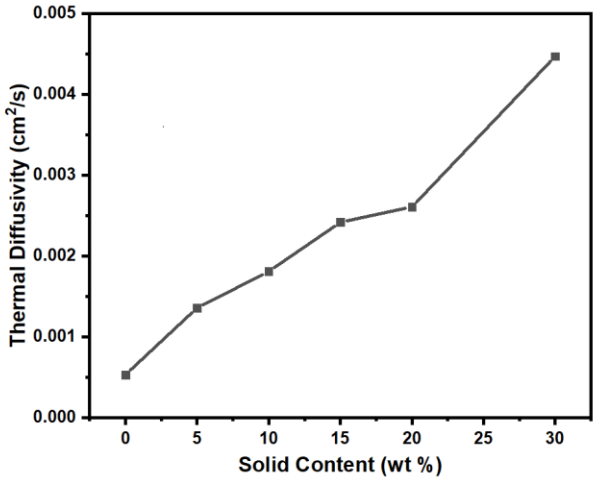

Figure 3: Thermal diffusivity of BN/silicone composites

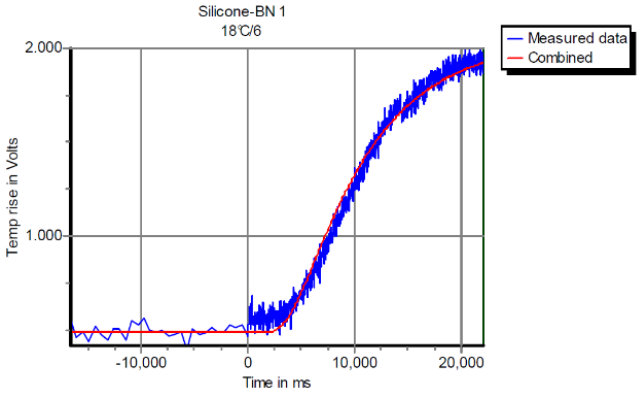

Figure 4: Standard LFA fitting for pure silicone rubber

All the samples are demolded from the mold and cut into standard 1-inch pellets for laser flash measurements. Then, both layers of the sample pellets are sprayed with graphite spray, which helps the sample absorb more energy from the laser pulse. The thickness of the coated sample l is measured with a vernier caliper, the density of the sample ρ is calculated from volume and weight measurement. The temperature of the sample T is controlled and read from a build-in temperature controlling oven inside the LFA. The heat capacity of the samples is determined from DSC (Differential scanning calorimetry) measurement.

DSC measurement is conducted with TA Instruments Q2000 Differential Scanning Calorimeter in CESI (Cornell Energy Systems Institute).

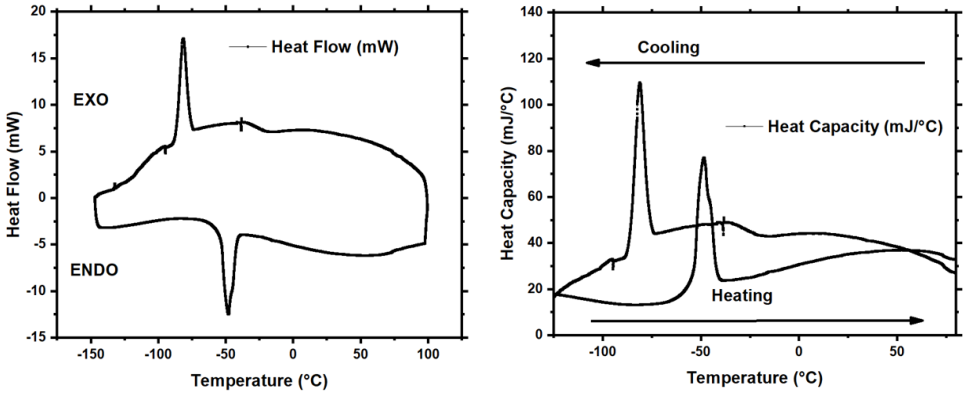

Figure 5: DSC heating scan and cooling curves for silicone rubber

The composite samples are heated from -150 ℃ to 100 ℃ at a constant heating rate of 5 ℃/min inside the capillary cell of the calorimeter under a nitrogen atmosphere. The sample cell is placed near a reference cell. Three runs are taken on average to minimize the noise. The results are shown in figure 5, and we can get heat capacity for the silicone rubber in this way.

3.2.3 Result Analysis

LFA can accurately and rapidly measure the thermal diffusivity of bulk samples like silicone/BN composite. With additional density and heat capacity LFA can give accurate results for thermal conductivity. From the result, we can see that the thermal diffusivity of the composite increases almost linearly with the solid content, which can be attributed to the rule of mixture[9]. When there are enough fillers in the matrix, fillers form an interconnected percolation network inside the matrix[10]. This percolated network will serve as a heat conduction pathway, enhancing the thermal transport inside the composite material.

However, adding too many small particles into the matrix can seriously harm the overall thermal diffusivity. When an alien inclusion like a nanoparticle is imbedded into the matrix, an extra interface is also introduced, leading to very high interfacial thermal resistance if the particle has very large relative surface areas.[11] Nonetheless, larger particles will make it much harder to make nanocomposite, and whenever a large particle is presented, it will lead to weaker mechanical properties because of strain focus in these areas. Making a mechanically sound and conducting composite depends on a delicate balance between solid content and particle sizes.[12]

3.3 Thermal diffusivity measurements for polymer blends

3.3.1 Sample preparation

Silicone-Glycerol polymer blends are provided by Professor Skov's group from the Technical University of Denmark. All the sample preparation steps for LFA are identical to the

sample preparation steps mentioned for BN/silicone composites. Dr. Liyun kindly provides heat capacity measurements for us.

For these samples, Sylgard 184 is a commercial two-part silicone kit from Corning, and Sylgard is mechanically blended with glycerol in a series of solid contents.

Table 1: Silicone-glycerol system formulation

Sample abbreviation	Sample name	Glycerol content (phr)	ZnO content (phr)
S184	Sylgard 184	0	0
S184G40	Sylgard 184 & Glycerol	40	0
S184G60	Sylgard 184 & Glycerol	60	0
S184G80	Sylgard 184 & Glycerol	80	0
S184G100	Sylgard 184 & Glycerol	100	0
S184G120	Sylgard 184 & Glycerol	120	0
S184G40W	Sylgard 184 & Glycerol	40	0
S184G60W	Sylgard 184 & Glycerol	60	0
S184G80W	Sylgard 184 & Glycerol	80	0
S184G100W	Sylgard 184 & Glycerol	100	0
S184G120W	Sylgard 184 & Glycerol	120	0
S184 5Z100	Sylgard 184 & nanosized ZnO (100 nm)	0	5
S184 1Z100	Sylgard 184 & nanosized ZnO (100 nm)	0	1
S184 5Z50	Sylgard 184 & nanosized ZnO (50 nm)	0	5
S184G40 5Z100	Sylgard 184 & Glycerol & nanosized ZnO (100 nm)	40	5

3.3.2 Sample measurements

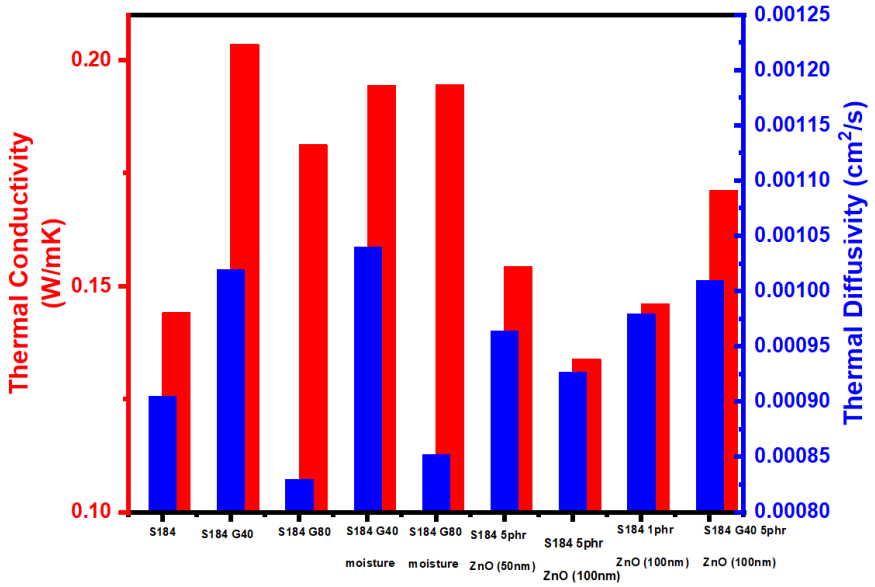

Figure 6: Thermal properties of glycerol/ZnO modified Sylgard 184

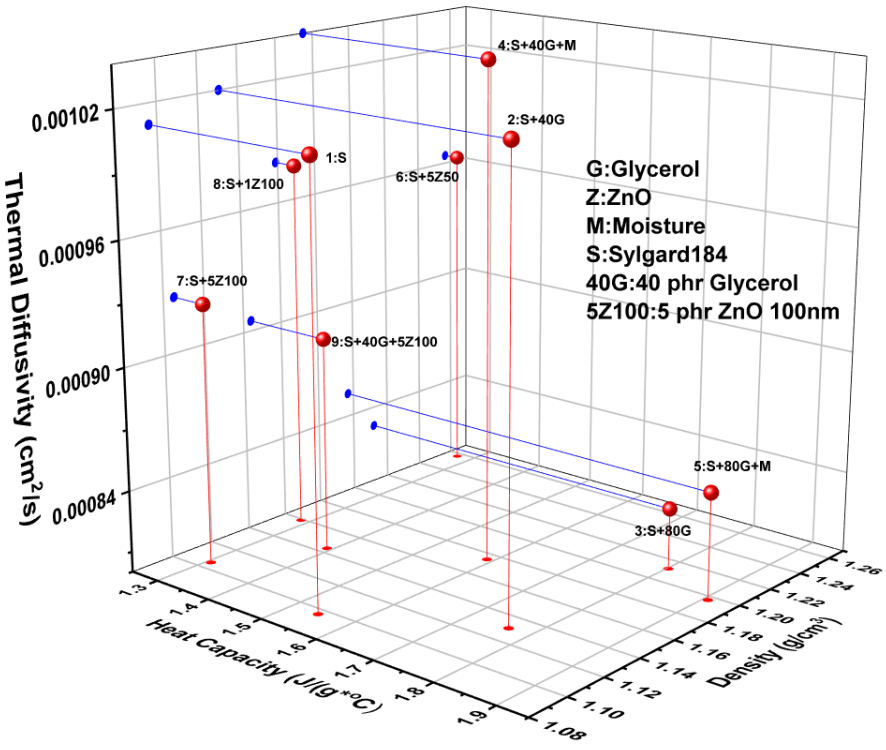

Figure 7: Contribution distributions towards thermal conductivity

Figure 6 and figure 7 illustrate the contribution from thermal diffusivity, heat capacity, and density towards thermal conductivity among different samples. The addition of glycerol drastically increases the overall heat capacity of the sample, which in turn increases the material's thermal conductivity. When considering a nanofiller for making a polymeric composite, we should always balance well between particle size and filler's solid content. Also, considering a solid content high enough can make percolate channels inside the matrix material, which drastically increases thermal conductivity.

Typically, we would see an increase in thermal conductivity because of an increase in thermal diffusivity, where thermal diffusivity defines how fast a material reacts to a change in temperature or heat transfer rate. For sample 3 and sample 5 have relatively high thermal conductivity. However, this contribution mainly comes from the significantly higher heat capacity of these two samples. The density between different samples only varies by a small margin, which means that either glycerol, ZnO, or moisture will significantly affect the density.

Bulk ZnO has much higher thermal conductivity than the silicone rubber used for these samples. However, 100nm nanosized ZnO has a very high interfacial thermal resistance, compensating for the increase of thermal conductivity by the inclusion of ZnO. It can be seen in the figure that the addition of ZnO nanoparticles is not helping with increasing the thermal conductivity of the samples. Furthermore, in some cases (like sample 7), the addition of nanoparticles is hurting the overall thermal conductivity of the composites.

Moisture is not increasing the overall thermal conductivity; it should be excluded when making a composite with higher thermal conductivity.

3.3.3 Result

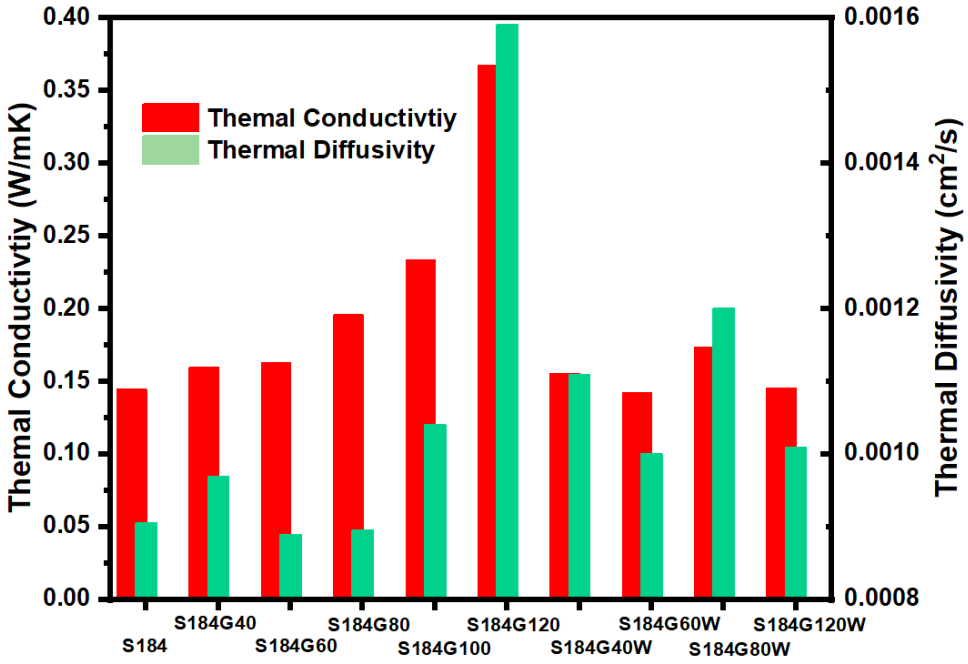

Figure 8: Thermal properties of Sylgard 184/glycerol blends

Results are summarized in figure 8, where W stands for moisture treatment. In conclusion, we can find that the addition of glycerol can improve the thermal conductivity of Sylgard 184 silicone rubber. The increase in thermal conductivity increases steadily as the solid content of glycerol increases. The composite's thermal diffusivity and thermal conductivity drastically increase as the solid content of glycerol increases from 100 phr to 120 phr, explaining that as more glycerol is introduced, an interconnected percolated network of glycerol is formed inside the silicone rubber matrix. Also, we found that moisture in the sample will adversely affect the thermal transport properties, which reinstate the importance of storing samples in dry conditions.

References

[1] Zhao, D., Qian, X., Gu, X., Jajja, S. A. & Yang, R. Measurement techniques for thermal conductivity and interfacial thermal conductance of bulk and thin film materials. *J. Electron. Packag. Trans. ASME* **138**, 1–19 (2016).

[2] Zhao, Y. H., Wu, Z. K. & Bai, S. L. Thermal resistance measurement of 3D graphene foam/polymer composite by laser flash analysis. *Int. J. Heat Mass Transf.* **101**, 470–475 (2016).

[3] Park, Y. H., Ku, D. Y., Ahn, M. Y., Lee, Y. & Cho, S. Measurement of thermal conductivity of Li 2 TiO 3 pebble bed by laser flash method. *Fusion Eng. Des.* **146**, 950–954 (2019).

[4] Min, S., Blumm, J. & Lindemann, A. A new laser flash system for measurement of the thermophysical properties. *Thermochim. Acta* **455**, 46–49 (2007).

[5] Shinzato, K. & Baba, T. A laser flash apparatus for thermal diffusivity and specific heat capacity measurements. *J. Therm. Anal. Calorim.* **64**, 413–422 (2001).

[6] Abdulagatov, I. M., Abdulagatova, Z. Z., Kallaev, S. N., Bakmaev, A. G. & Ranjith, P. G. Thermal-Diffusivity and Heat-Capacity Measurements of Sandstone at High Temperatures Using Laser Flash and DSC Methods. *Int. J. Thermophys.* **36**, 658–691 (2015).

[7] Vozár, L. & Hohenauer, W. Flash method of measuring the thermal diffusivity a review. *High Temp. - High Press.* **35**–**36**, 253–264 (2003).

[8] Lunev, A., Zborovskii, V., Aliev, T., Heymer, R. & Vilkhivskaya, O. PULsE: An open-source software for laser flash analysis. *Softw. Impacts* **6**, 100044 (2020).

[9] Patil, A. & ShashaVali, S. Estimation of thermal conductivity of short fiber composites. *Mater. Today Proc.* (2021). doi: 10.1016/j.matpr.2020.12.972

[10] Xu, W., Zhang, Y., Jiang, J., Liu, Z. & Jiao, Y. Thermal conductivity and elastic modulus of 3D porous/fractured media considering percolation. *Int. J. Eng. Sci.* **161**, 103456 (2021).

[11] Song, D. X., Ma, W. G. & Zhang, X. Thermal conductivity in highly loaded metallic nanowire-dielectric composite: Effect of percolation network. *Chem. Phys. Lett.* **731**, 136630 (2019).

[12] Nuernberg, R. B., Machado, N. M. P., Malki, M. & Neyret, M. Electrical behavior of RuO2-glass composites: The effect of RuO2 particle size on the percolation threshold. *J. Nucl. Mater.* **546**, 152777 (2021).

4. FDTR

Modern microelectronic devices and thin-film materials impose new challenges in nanoscale heat transfer. As industrial and academic areas demand smaller and smaller device sizes, a fundamental understanding of nanoscale heat transfer is becoming increasingly critical.[1] Optical thermal measurement technique makes the measuring speed orders of magnitude faster , and the length scales orders of magnitude smaller. Among which the pump-probe system is one of the most common techniques for optical thermal measurements.[2-4] For such a system to work, first, the pump laser reaches the sample surface and heats the sample, which leads to changes in the sample properties like reflectivity, absorptivity, and transmissivity. Then the probe laser arrives at the same spot and transfers the information of those changes in physical properties back into a detector. A delay stage is usually deployed to cause a time delay in laser reaching the sample surface, which helps study the physical process evolution.[5]

FDTR is thermal property microscopy, which utilizes two lasers (pump and probe lasers, figure 9) to measure the samples' thermal properties. The periodically modulated pump laser locally heats the sample, and the probe laser detects the surface reflectivity of the sample, which can be used to calculate the thermal properties of the sample with models.[6,7]

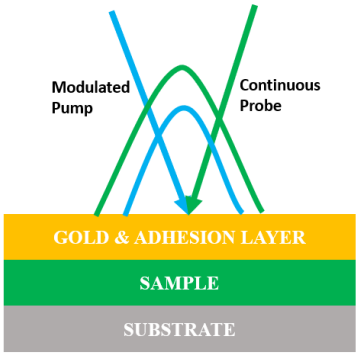

Figure 9: Pump-Probe system for FDTR

Different groups have proposed different setups of the FDTR system. For each FDTR system, the setup is different due to the sample &equipment requirement, optical path setup, and laser differences. However, the key of FDTR is always the same – a pump-probe system with frequency modulation.

Professor Schmidt[8] built a pump-probe laser system that employs a tunable Ti: Sapphire laser and a bismuth triborate (BIBO) crystal for their measurements, where measurements of various liquid samples are made possible. This is a prototype of the FDTR system, where the pulsed laser is divided into pump and probe pulses with BIBO crystals. Their improved model of the FDTR system uses two separate CW (continuous wave) lasers instead of a pulsed laser.[9] Even though pulsed laser setup makes it easier to switch between TDTR system and FDTR system, CW lasers system makes the whole setup much simpler and easier to control.[10]

His student Yang[11] set up an FDTR system based on a 785 nm pump laser and a 532 nm probe laser. He demonstrated that, when paring the FDTR system with a precision X-Y Piezo Stage and auto fitting programming, it is possible to make a 2D mapping of thermal properties of a sample. Their setup has improved the signal-to-noise ratio and pushes the limits of the FDTR system beyond simply measuring a single sample spot.[12] This makes FDTR more suitable for analysis in microelectronic devices.

Professor Malen[13] also set up a broadband FDTR, where modulated 488 nm CW pump laser heats the sample, and 532 nm CW probe laser detects the thermoreflectance and yields the temperature response to the sample surface. They applied additional modulation for the reflected probe beam and a novel heterodyne approach to push the frequency higher (up to 200MHz) and increase the signal-to-noise ratio.

4.1 FDTR Component

4.1.1 Pump and Probe laser

Both two lasers are CW (continuous wave) lasers, and both are purchased from Coherent Inc. The Genesis MX488-1000 STM 488 NM CW laser is the pump laser, which heats the sample and generates a thermoreflectance in the sample surface area; the Verdi G2 532 nm CW laser is the probe laser, which detects the thermoreflectance caused by the pump laser.

4.1.2 Isolator

There is a compatible isolator for each laser, which prevents the refection of the laser back into the pump and probe laser. Both isolators are from Conoptics Inc., where model 711A 532 nm isolator and model 711C-3 488 nm isolator are incorporated into the FDTR system.

4.1.3 Half waveplates and quarter waveplate

All the half waveplates will change the polarization of the laser passing through it. Each laser is equipped with a half waveplate with the same wavelength (WPH05M-532 for 532 nm laser and WPH05M-488 for 488 nm laser). 532 nm quarter-wave plate (WPQ05M-532) is used before the objective. All three waveplates are purchased from Thorlabs.

4.1.4 Balanced photodetector

Model PDB450A-AC photodetector from Thorlabs receives the reflected laser and converts it into signals. The balanced photodetector utilizes two receivers and enhances the signal-to-noise ratio.

4.1.5 EOM

Model HF2LI lock-in amplifier is purchased from Zurich instruments, detecting the phase lag between two lasers and providing an interface for us to control the system. Model

350-160-01 EOM (electro-optical modulator) is purchased from Conoptics Inc., which modulates the pump laser.

4.1.6 BS and PBS

Beam splitter (BS025, Thorlabs) split and guild the laser, polarizing beam splitter (PBS201, Thorlabs) adds polarization to the laser while split and guild the laser.

4.1.7 Objective

A 20x Microscope objective (MY20X-804, Thorlabs) is used in the system to focus the laser. Other magnifications of the objective are interchangeable with this one depending on the sensitivity requirements.

4.1.8 Delay stage

Two mirrors guild the laser to a more extended pathway, which acts as a delay stage in the system.

4.1.9 Band filters

532 nm bandpass filter (#65-155, Edmund) blocks out 488 nm laser while allowing 532 nm laser passing through it. 488 nm bandpass filter (#65-147, Edmund) blocks 532 nm laser while allowing 488 nm laser passing through it.

4.1.10 Piezoelectric translation stage

Model P-545.3C8S piezoelectric translation stage from Physik Instrumente can maneuver the sample with high precision (resolution 0.1 microns, maximum range 200 microns).

4.1.11 CCD camera

Model DCU224C CCD camera from Thorlabs can give the lasers and samples images, which helps in laser alignment. A typical digital photo captured by a CCD camera is shown in figure 10.

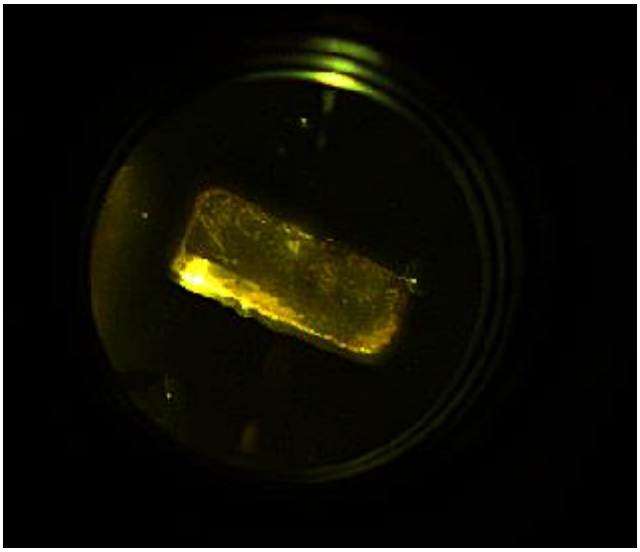

Figure 10: A digital photo captured by CCD camera

4.1.12 Power meter

The model 843-R power meter is purchased from Newport, which gives accurate readings of the laser power strength.

4.2 System setup

Our FDTR system utilizes two continuous-wave (CW) lasers: a 488nm pump laser and a 532nm probe laser. The pump beam first passes into an optical isolator, which prevents the back-reflection of the beam into the laser cavity. Back-reflection can lead to instabilities in the laser output power. The pump beam travels through and is modulated with an electro-optic modulator (EOM). This beam is then guided with mirrors and focused on the sample with a 20x

microscope objective, which creates a periodic heat flux with a Gaussian spatial distribution on the samples. The probe beam travels through a BS after an optical isolator and is then aligned coaxially with the pump beam. The beam is split with PBS and focused on the pump spot to monitor the periodic fluctuations in reflectivity at the sample surface caused by the oscillation from sample temperature. Then, the post-sample beams are reflected in the PD. The PBS also divides some parts of the probe laser to a delay stage and then to another receiver of the PD. The power of the laser going into the two receivers should be identical to minimize the noise. Fine balancing is performed by adjusting the half waveplate until the noise is minimized. A bandpass 488nm filter is placed before the photodetectors block scattered pump light, which would otherwise overwhelm the thermal signal. The sample is coated with a thin film of gold with a thickness of 80-100 nm. Gold is chosen to maximize the coefficient of thermoreflectance at the probe wavelength. A thin layer of titanium adhesion can be deposited before gold deposition if there is insufficient adhesion between the gold and the sample. The sample is mounted on a closed-loop piezoelectric translation stage with a 200 μm scanning range in the x, y, and z directions. The lock-in amplifier records the amplitude and phase data, where the phase data is obtained with increasing frequencies. A layer-structured model is used for fitting and calculating the thermal properties.

4.3 Alignment

Alignment is of paramount importance in running the FDTR system, and every single optic must be perfectly aligned to get stable and robust signals. In comparison, a single misalignment in the laser path can lead to colossal noise or catastrophic failure in the measurements. Fine-tuning of the system and troubleshooting must be done before the start of each measurement cycle.

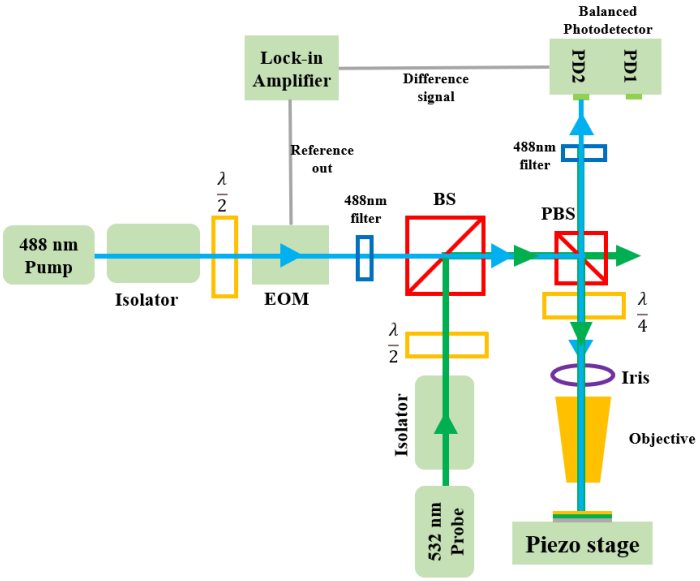

Figure 11: First FDTR setup

Before getting our system to work, our FDTR setup experienced two significant changes to solve the major issues.

In the first setup, both pump and probe lasers are guided into the coaxial pathway by the first BS. Then, these two beams are deflected and polarized with the PBS, where the deflected laser moves toward three sample stages. After focusing with a microscope objective, the two lasers are reflected towards PD, where a 532 nm filter filters out the probe laser.

In the first setup, only one receiver of the PD is used for detecting the signal. However, a balanced photodetector requires two beams to balance out the noise, and there is not enough room in the current pathway for that comparison beam.

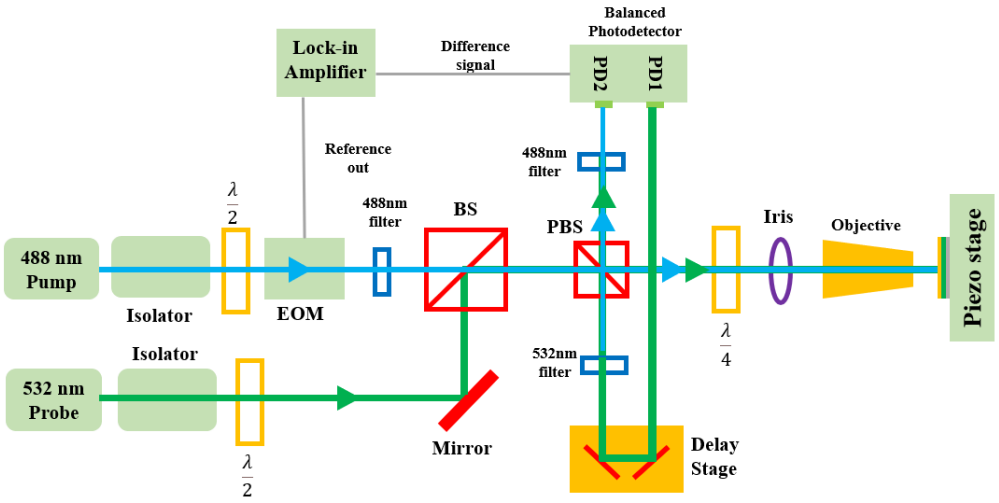

Figure 12: Second FDTR setup

On the second setup, a delay stage is used to deflect and generate an equal optical pathway length, where the two lasers should pass an equal distance (equation 6) after passing through the PBS. With a pump laser on PD2 and probe laser on PD1, the balanced PD can minimize the noise during measurement.

$$L_{PBS-S} + L_{S-PD} = L_{PBS-D} + L_{D-PD} \tag{6}$$

Where L_{PBS-S} is the distance from the center of PBS to the surface of the sample, L_{S-PD} is the distance from the sample surface to the receiver (PD2) of PD, L_{PBS-D} is the distance from PBS to the delay stage, and L_{D-PD} is the distance from delay stage to the receiver (PD1) of PD.

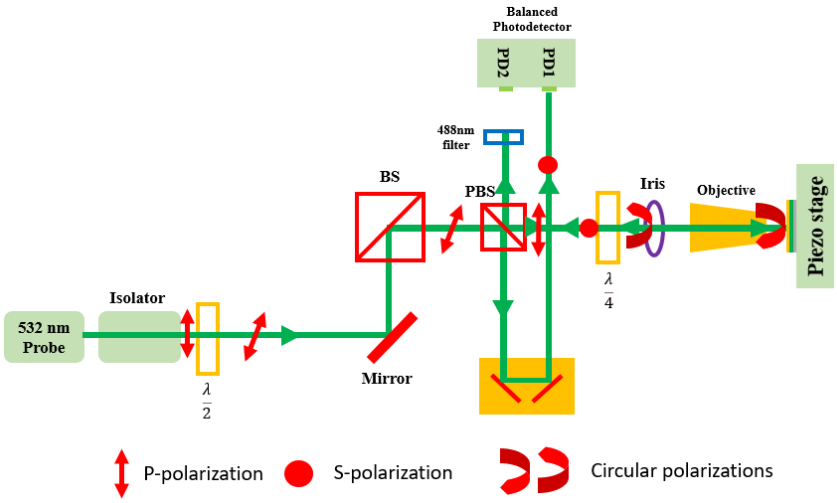

Figure 13: Polarization of light align the path

We want to change from the second setup to the third setup because we want to maximize the s-polarization output towards the photodetector. When coming out of the laser device, both pump and probe beams are vertically polarized (p-polarization) beams. Because there is a 5% uncertainty in polarization for the lasers, we need to use a half-wave plate ($\frac{\lambda}{2}$) to correct this uncertainty and make sure that the pump beam is perfectly p-polarized. EOM can also change the polarization of the beam. However, in our setup, we only want to maximize p-polarization output. Thus, the EOM row angle is carefully chosen to allow the vertically polarized beam path through without any alteration of the polarization. A balanced photodetector requires a reference beam to minimize the noise, where we found in our experiments that equal beam strength at the two receivers can minimize the noise. We need to adjust the half-wave plate for the probe laser to allow a mixture of p and s-polarization of the probe beam to come out of the half-wave plate.

Moreover, since PBS only allows the p-polarization beams to continue travel to the sample while screens out all the s-polarization in our beam pathway, both the pump and probe beam will only have p-polarization after coming through the PBS. We are doing this step

because it is much easier to control the strength of two lasers, and it makes it easier to get minimized signal noise. Two p-polarized lasers are aligned perfectly after passing through the PBS, and they should always be coaxial in the following beam path. The quarter-wave plate ($\frac{\lambda}{4}$) circularly polarizes the light, so we have circular polarization before entering the objective and reaching the sample. The beams reflected by the sample have a π phase shift that reverses the polarized direction. These reversed circularly polarized beams will pass the quarter-wave plate and turn into horizontally polarized beams (s-polarization). The circular polarizations have two different directions before and after they reach the sample. As shown in the figure, the circular polarization with clockwise direction is the beam coming towards the sample and the circular polarization with counter clockwise direction is the beam reflected from the sample. Moreover, the circular polarization with counter-clockwise direction is the beam reflected from the sample. The PBS then redirects the s-polarization towards the PD. One must carefully choose the angle value for both the half-wave and quarter-wave plates, as we only want p-polarization to go into the sample beam path and s-polarization to come out of the reflected beam path. If the pump beam is a mixture of s-polarization and p-polarization, the s-polarization will be screen out by the PBS and only leave behind the p-polarization in the pre-sample beam path, making the beam strength and signal much weaker.

Our final setup can both minimize the noise in the measurement while obtaining maximized signal strength. The final FDTR system is shown in figure 14.

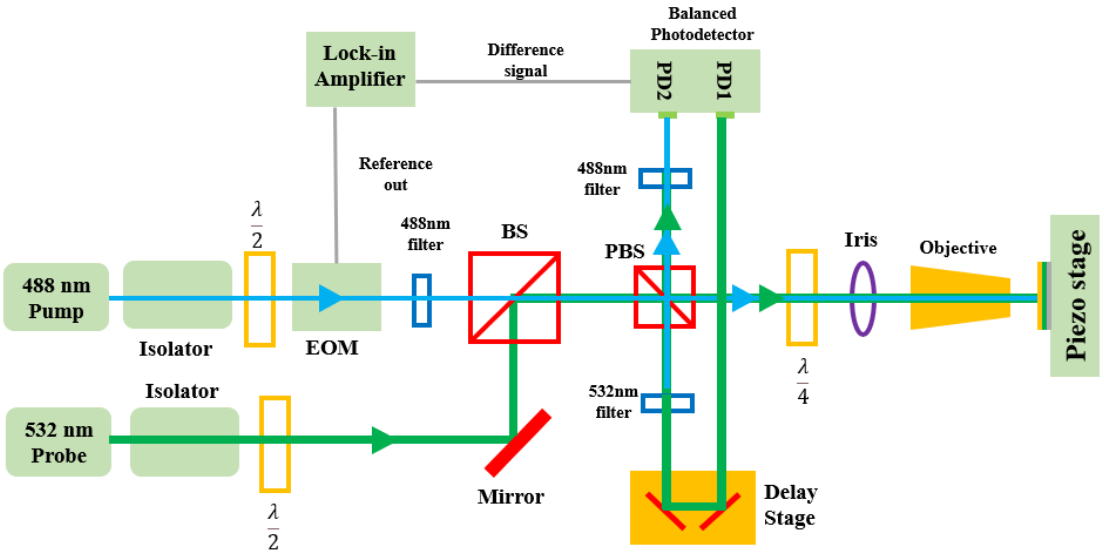

Figure 14: FDTR setup (final version)

4.3.1 Laser source alignment

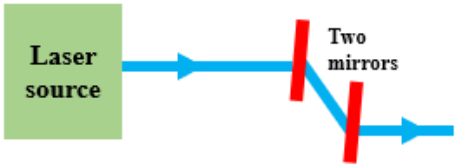

Figure 15: Two mirror adjustment

When mounting the laser onto the water-cooling stage (probe laser) and lab jack (pump laser), the joints and connections between the laser and stage will inevitably cause a shift in laser angles. Even without stages, some lasers are not parallel to the optical table when generated. A set of two mirrors can correct this deviation in the laser angle. First, deflect the laser light with the first mirror; try to deflect it at a large angle to have enough space for a second mirror. After fixing the first mirror, place the second mirror in front of the first mirror, rotate the mirror until the laser is parallel to the one that comes out of the laser source. Then, using a set of irises, take turns adjusting the left-and-right button on the two mirrors until the laser are perfectly

parallel to the laser from the laser source. Then take turns adjusting the up-and-down buttons on the mirror to adjust the height of the laser until the laser is parallel to the optical table. When adjusting one button on the mirror in a specific direction, one should adjust the button on another mirror in the opposite direction.

4.3.2 Objective alignment

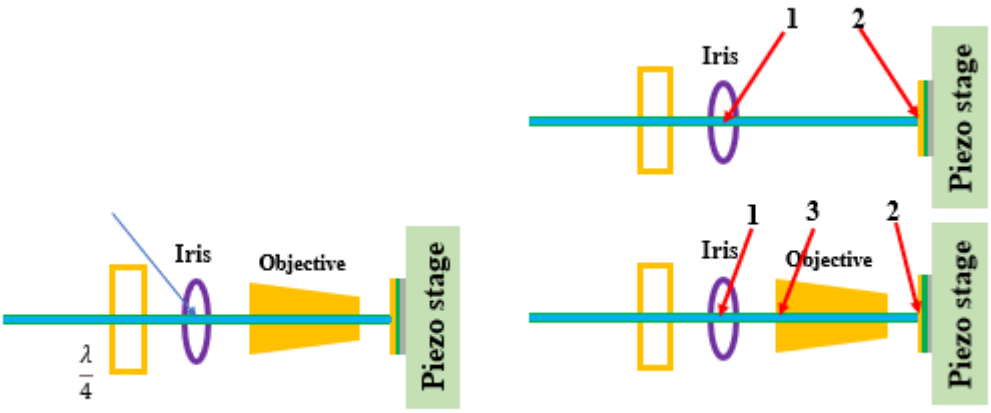

Figure 16: Schematic of objective alignment

Dismantle the objective and mark the sample surface where the laser spot land is marked "2" in the figure. The reflected light from the sample on the iris is marked as "1". When putting back the objective, first make sure the height of the objective is in the right place. When looking at the objective from the back direction (marked as "3" in the figure), the incoming laser and reflected laser should be co-axial. Here a fining tuning of the position of the objective should be performed before fixing the height and angle of the objective. After fixing the height of the objective, make minor adjustments to the objective's angle to make sure the reflected laser does not move away from "1".

4.3.3 BS alignment

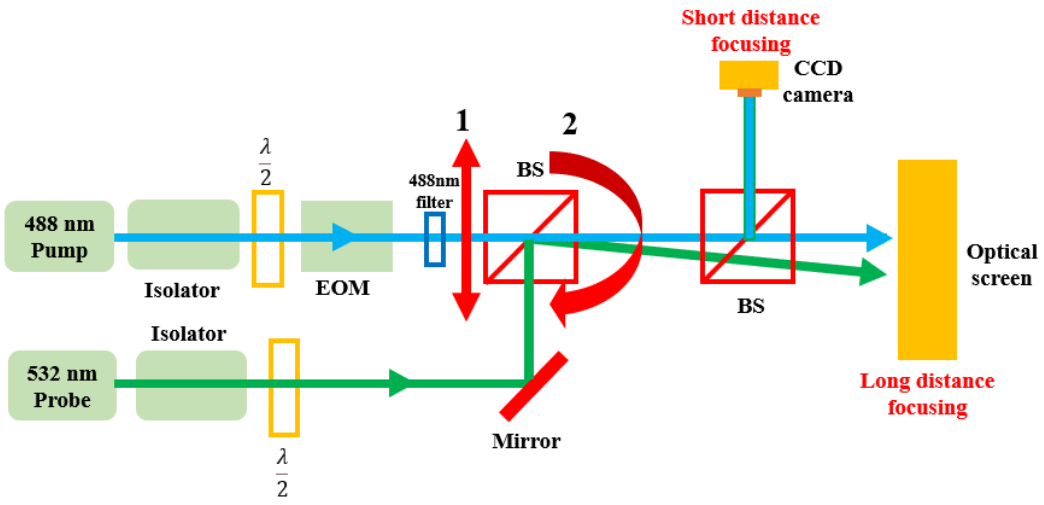

Figure 17: Schematic of BS alignment

The role of BS is to deflect and align the two laser beams to be coaxial. In order to perfectly align the two lasers with BS, an optical stage is used for fine-tuning (up-and-down as shown with the double-headed arrow 1). First, remove all the optics that can block or change the laser pathway, put a screen against the wall where the two lasers land. This step will be referred to as long-distance focusing in the following section. Then use another BS to deflect part of the laser pathway so the CCD camera can image the laser positions. This step will be referred to as short distance focusing on the following section.

To align the BS:

First, adjust the stage marked as “1”, then adjust the angle of BS marked as “2” to compensate for that distance change in the CCD camera and try to make the two lasers coaxial. If the two lasers are coming apart in the long-distance focusing in this way, we will go the opposite way for stage adjustment.

Second, go the opposite way for stage “1” and compensate the distance change to make the short distance focusing perfect.

Third, make the adjustments in such two-step adjustment in turns until the two beams are coaxial both at short distance focusing and long distance focusing.

4.3.4 EOM Alignment

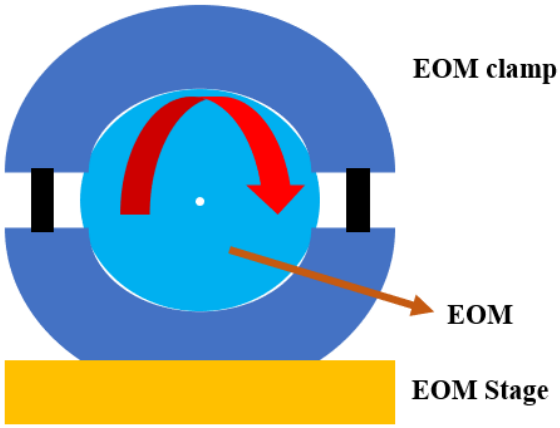

Figure 18: Schematic of EOM alignment

The adjustment on the EOM is one of the most complicated steps in FDTR alignment steps. We should pay attention to the position, angle, height, and rotation of the EOM simultaneously. Even a minor misalignment in EOM will lead to a significant deviation in the fitting curve.

For alignment, first set the bias voltage to 0, turn it off, disassemble all the optical cages on the EOM, put it aside from the EOM stage & clamp set, and then mount on an EOM alignment tool onto the cage. Second, put a power meter after the EOM to measure the power of the laser that comes out of the alignment tool. Adjust the height of the EOM stage first, then adjust the four screws on the EOM clamp to fine-tune the EOM position. Repeat this process until the power output is maximized (the laser power should be the same or slightly higher before and after the alignment tool). After this, put away the alignment tool and place back the

EOM. Rotate the EOM within the EOM clamp slowly until the power output reaches the maximum value. Finally, tighten up all the screws for the clamp and turn on the bias voltage for other alignment or measurements.

4.3.5 PD Alignment

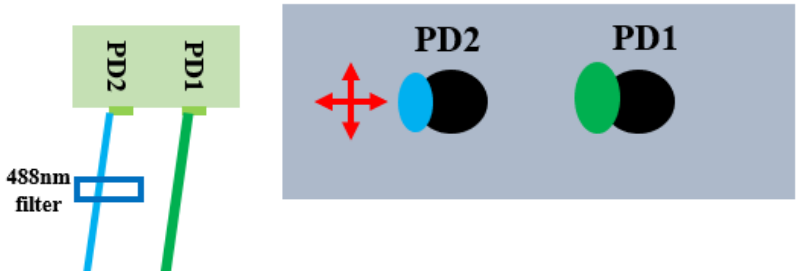

Figure 19: Schematic of PD misalignment

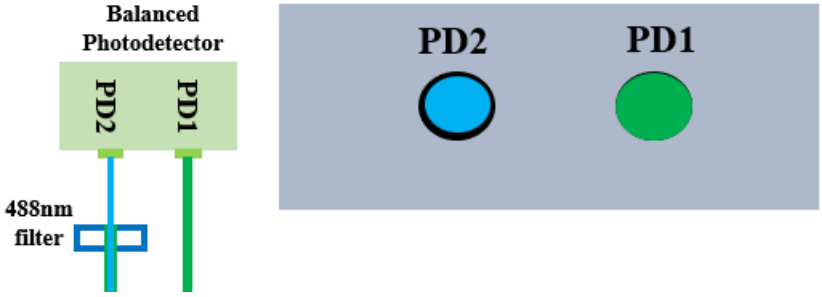

Figure 20: Schematic of correct PD alignment

PD adjustment is crucial in obtaining a maximized signal, affecting the noise level significantly.

First, one should make sure the reflected laser beams are fixed in certain positions. When changing the distance of the sample and changing the size of reflected beams, the centers of the reflected beam should not move. This step is because, during fine-balancing of the system (maximizing the signal output), PD position and sample distance will change to find the maximum signal. We will need the beam to be fixed to finish the fine balancing step. For the fixed position of reflected laser beams, the objective will have to be fixed first. Then by

changing the distance of the sample to the objective, one can observe the dynamic changes of the reflected laser beam when it changes size and shape. If the laser beams are too bright or too small to see, ND filters and a CCD camera can be used to do the fine-tuning. If the laser beam center keeps shifting places, one can alter the angle of PBS to correct the shift until the reflected beams are fixed in place.

The second step is to adjust the position, angle, and angle of the PD. For fine-tuning of the PD, an x-y axis stage with rotation is used for tuning the height, position, and angle of PD. It can be seen from the figure that if the incident laser beams are tilted or at an angle, the PD will only receive a fraction of the signal from the reflected lasers. Moreover, if the reflected lasers are at an angle, the reflected lasers will deform into an oval shape, significantly influencing the signal strength and quality and leading to considerable noise in FDTR measurements. To set the PD in the proper position, we should first find the PD position where the two lasers are vertically incident to the PD receivers. Remove the PD from the stage and install a CCD camera; by moving the position of the CCD camera, we will see the shape of reflected laser beams keep shifting from oval to a circle. Mark the place where reflected lasers are circles and install PD on that position. Then, maximize the signal reading from PD by adjusting the PD's height, position, and angle (fine-tuning). During this step, one should take turns adjusting the position of the sample stage and the PD stage, in which way one can maximize the signal and minimize the noise.

4.3.6 PBS alignment

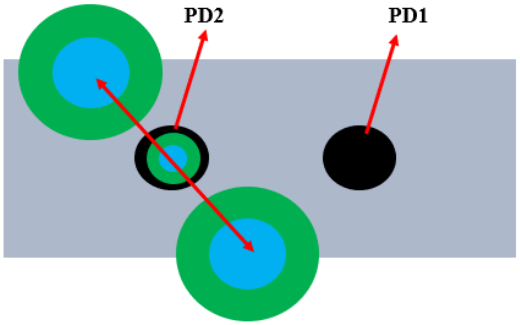

Figure 21: Schematic of PBS misalignment

Figure 22: Schematic of Correct PBS alignment

When adjusting the PBS, first make sure all the other parts mentioned before are aligned. Then, put an optical ruler before the PD. Adjust the angle of PBS (up-and-down) to make sure the height of the reflected laser is the same everywhere else. After this, adjust the left-and-right angle of PBS to fix the laser. The correct method for this is constantly changing the sample distance from the objective, which causes the reflected beam to change focus point (the size of beams on the PD will change, shown in figure 21). Adjust the PBS while trying this method until the reflected beams will not shift their places, as shown in figure 22. This method is also another way to examine whether the objective is perfectly aligned. If PBS adjustment fails to immobilize the reflected laser on the PD, it means the objective needs a re-adjustment.

4.3.7 Sample Alignment

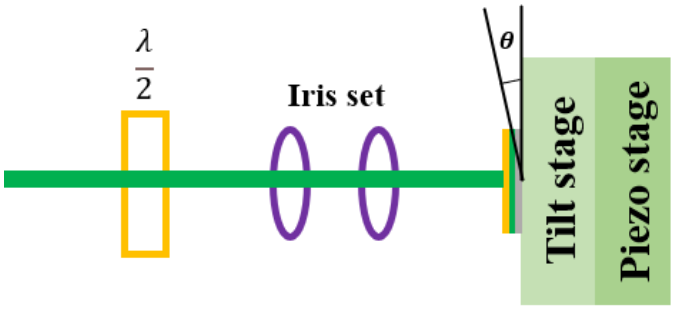

Figure 23: Tilt stage alignment

The Piezo stage can be equipped with a tilt stage for samples with a tilted angle or uneven surface. When pairing a tilt stage with a piezo stage, the sample can freely move in the x-y direction and rotate in different directions (x-axis and y-axis). When mounting the tilt stage, remove the objective and install a set of irises. Adjust the sample until the reflected light can go back in the same pathway they come through the irises. If the reflected light passes through the first iris while lands on the corner of the second iris, it means the sample is tilted. Adjust the tilt stage until the reflected laser can pass through the irises.

4.3.8 Co-axial check

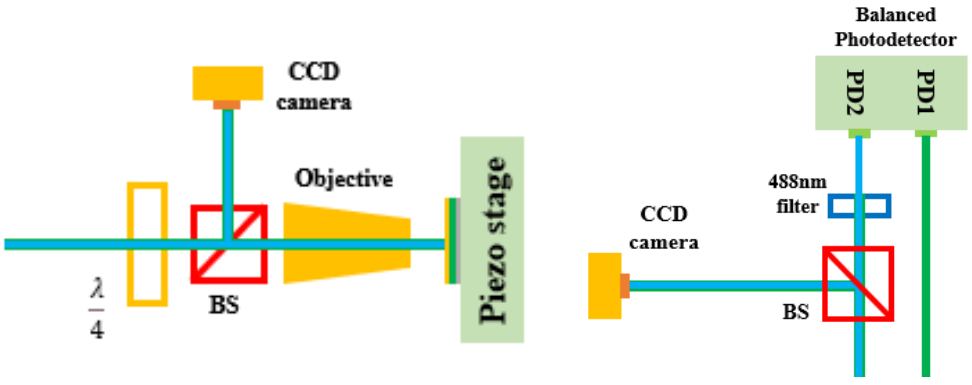

Figure 24: Schematic of Co-axial check

There are always all kinds of influences and noise from the environment – a change in the temperature, vibration from the table, mechanical failure or damping of stages, or instability from the lasers. These factors will all contribute to the shift of beam alignment and measurement noises. Thus, after the alignment of all the optics, a final check is necessary before each measurement run to make sure the system is perfectly aligned.

A two-step final checking can ensure the quality of beam alignment. First, deflect a part of the incoming laser towards the sample stage, observe the laser alignment with a CCD camera. Then, deflect a part of the laser before the PD, also observe the laser with a CCD camera. If both checking points are perfectly aligned, like shown in the digital picture, then the environmental influence is tolerable for the system. If either of the two checkpoints is not perfectly aligned, we need to check the BS, BS stage, objective, and mirrors.

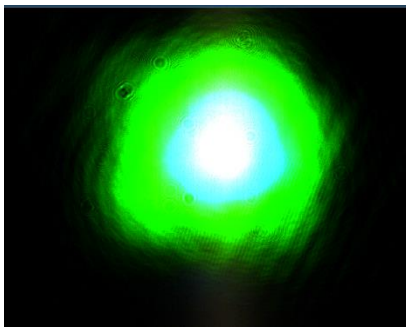

Figure 25: Beam alignment in CCD camera

Figure 25 shows how a perfect co-axial alignment of two lasers is like in the view of a CCD camera.

4.4 Parameters

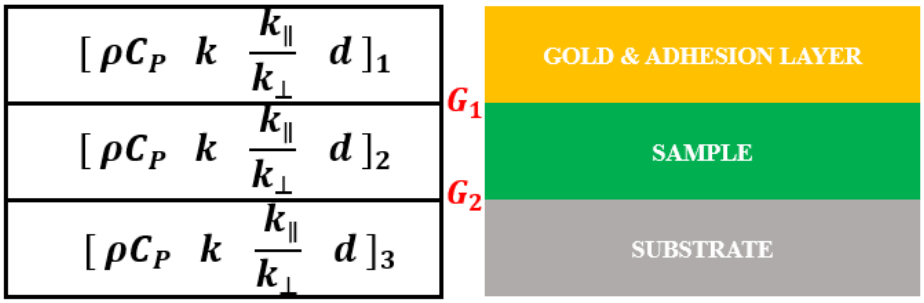

Figure 26: Models in FDTR system

In our model, the parameter matrix consists of a three-layer structure. The topmost layer is the gold adhesion layer which maximizes the coefficient of Thermoreflectance at 532nm (probe wavelength). For samples with insufficient adhesion to the transducer layer, a thin layer (~5nm, titanium) of the adhesion layer is utilized for interfacial adhesion enhancement. The middle layer is the sample, whose both layers should be homogeneous and smooth enough (roughness<20nm). A substrate layer is used for supporting the sample if the sample does not have mechanical strength. If the sample is thick enough (>1 μm), laser dots cannot penetrate the substrate layer, and the system can ignore the influence from the substrate.

For each layer, the model requires four parameters – volumetric heat capacity, thermal conductivity, anisotropy (k in-plane/k out-of-plane), and thickness of the layer, respectively. Between every two layers, an interfacial conductance G is also required in the model. In a typical measurement, all the known properties should be used as input in this model, and the maximum number of unknown parameters the model can fit is 2.

Because in our setup, we only use a very thin layer of titanium adhesion layer (5nm) and the transport properties between gold and titanium are similar, we can consider the gold and titanium all together as a single transducer layer.

4.4.1 Spot size

4.4.1.1 Knife-Edge Setup

$$f(x) = a_1 \times \exp\left[-\left(\frac{x-b_1}{c_1}\right)^2\right] \quad (15)$$

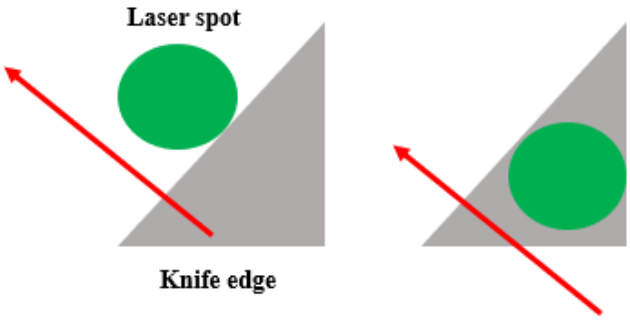

Figure 27: Knife edge spot size measurements

A very sharp knife is used for blocking the laser, where the power of the unblocked part of the laser is measured with a power meter. The reflected laser beams are deflected and guild into a CCD camera to make the fine-tuning much easier.

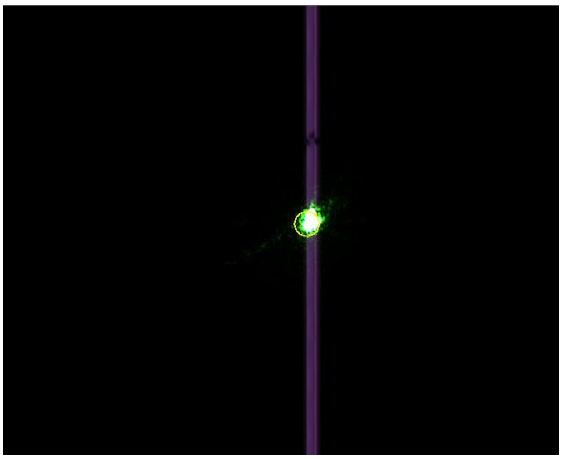

Figure 28: Knife edge spot size in CCD camera

In a typical spot size measurement, the piezo stage slowly moves the knife edge towards the laser beam until the knife edge is tangent to the beam spot and marks down the power readings from the power meter. Then move the piezo stage forward slowly (5μm per stop).

During each stop, mark down the power readings from the power meter. Using the distance interval and power reading, apply Gaussian fitting with the MATLAB package, where the fitting function is listed in equation 7.

Multiple measurements are taken in order to get the most accurate (smallest) beam size.

Table 2: Laser spot size Guassian fitting

532 nm laser spot size Guassian fitting									
Measurement	1	2	3	4	**5**	6	7	8	9
c_1 value	4.327	3.038	3.671	3.648	**2.698**	2.961	3.128	4.061	5.165
488 nm laser spot size Guassian fitting									
Measurement	1	**2**	3	4	5	6	7	8	9
c_1 value	3.485	**3.065**	3.515	3.655	3.245	3.293	3.394	3.539	3.485

Because we are selecting the focal length using the CCD camera, it is very tough to determine the actual focus point as the laser spot becomes too small to distinguish differences (shown in figure 28). Thus, multiple runs are required for getting the most accurate spot size measurements. As we know, that spot size is equal to $2c_1^2$, the smaller the c_1 is, the smaller the spot size is. For 532 nm laser, the smallest c_1 is 2.698, and for 488 nm laser, the smallest c_1 is 3.065. As a result, our measured spot size for the 20x objective is 5.775 μm.

4.4.1.2 Beam Profiler

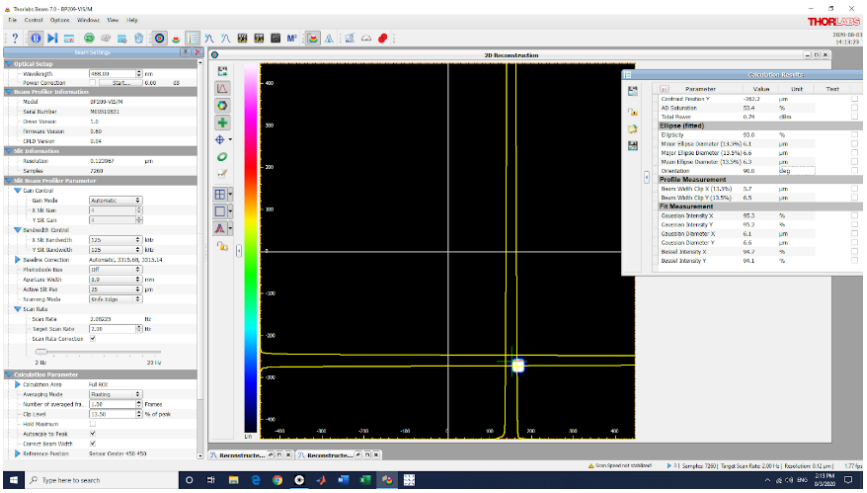

Figure 29: Beam profiler interface

For the beam profiler, it is effortless to measure. For measurements, we only need to guild the laser into the cavity of the beam profiler, and its interface will help do the calculation.

For laser spots with Gaussian intensity distribution patterns[12]

$$I(r) = \frac{2A_0}{\pi\omega_0}\exp\left(\frac{-2r^2}{\omega_0^2}\right) \tag{16}$$

Where A_0 is the laser power, ω_0 is $\frac{1}{e^2}$ radius.

The power recorded with a photodetector is[12]

$$P(x) = \frac{2A_0}{\pi\omega_0}\int_{-\infty}^{\infty} dy \exp\left(\frac{-2r^2}{\omega_0^2}\right)\int_{-\infty}^{x} dx \exp\left(\frac{-2x^2}{\omega_0^2}\right) \tag{17}$$

However, the signal is unstable, and the results shift a lot (>20%), making this method less reliable. Moreover, the first method using knife edge is the most accurate measurement for spot sizes.

4.4.2 Volumetric Heat capacity

The heat capacity of the samples is measured with TA Instruments Q2000 Differential Scanning Calorimeter in CCMR. The density of the samples is measured by dividing mass by

volume. For reference samples, the heat capacity for glass, silica, and gold are referred to as literature values.

4.4.3 Thickness

The thickness of the samples is measured with P7 and P10 profilometers in CNF. Each sample is taken in three different spots for thickness measurement and an average of three runs for each measurement.

4.4.4 Thermal conductivity of transducer layer

Wiedemann-Franz law converts electrical conductivity into thermal conductivity.

$$\frac{k}{\sigma} = \frac{3k_B^2 T}{2e^2} \tag{18}$$

$$\frac{k}{\sigma T} = Lorenz\ number\ (L) \tag{19}$$

Where k is thermal conductivity, σ is electrical conductivity, k_B is Boltzmann constant, T is the temperature and L is Lorenz number. For gold, the Lorenz number at 273K is $2.35 \times 10^{-8} \Omega W/k^2$.

The electrical conductivity of the samples is measured with Cascade CP06 Four Point Probe Setup in CCMR. From equation 10 and equation 11, the electrical conductivity values can be converted to thermal conductivity values. The measured value for the thermal conductivity of our gold layer is 193W/mK.

4.4 Sample preparation

4.54.1 Sample pretreatments

4.5.1.1 Flat thin film samples

For flat thin-film samples, there is not special pretreatment required. The surface topology can be determined using an optical microscope （Richter Optica, Model U2 biological microscope）and P7 profilometer. If the surface is flat and the roughness is around or less than 10 nm, the sample can be directly stuck onto a glass substrate with Loctite or Crystalbond adhesive. If an unevenness is generated from the adhesives, tilt stage examination should be done before any measurements.

4.5.1.2 Bulk solid samples

Chart 3: Diamond lapping

Grit Size (μm)	Name
30	LF30D Diamond Lapping Sheets, Thorlabs
6	LF6D Diamond Lapping Sheets, Thorlabs
3	LF3D Diamond Lapping Sheets, Thorlabs
1	LF1D Diamond Lapping Sheets, Thorlabs
0.02	LFCF Final Diamond Lapping Sheets, Thorlabs

D50-FC/APC polishing discs are purchased from Thorlabs, Crystalbond adhesives (Crystalbond 509, Crystalbond 555, Crystalbond 590) are purchased from Electron Microscopy Sciences. Depends on the properties of samples, we should wisely choose the adhesive. (Data from Electron Microscopy Sciences[15])

Chart 4: Properties of Crystalbond adhesives

	509 Crystalbond	555 Crystalbond	590 Crystalbond

Softening point/℃	71	52	125
Flow point/℃	121	54	150
Viscosity/cps	6000	500	9000
Solvent	Acetone	Water	Methanol

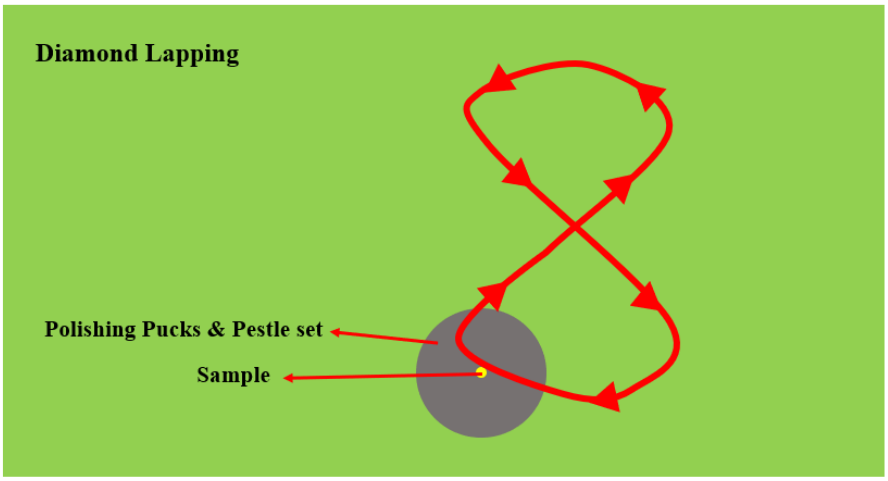

Figure 29: Schematic of diamond lapping polishing technique

A set of polishing pucks and pestles are used for polishing samples with uneven surfaces or shapes. First, cut the sample into smaller, processable pieces, which should be fitted with the size of the polishing pucks. Then, select an appropriate Crystalbond adhesive (based on the properties and working temperature of the sample), melt the adhesive, and attach the sample onto the pestle with the adhesive. After solidification of the adhesive, assemble the pestle into the polishing puck. Then, begin with 30 μm lapping paper, keep drawing "8" shape on the lapping without putting pressure on the sample. For each run of polishing, it takes 5 to 10 minutes until the friction will drastically decrease. Then, in such a manner, polish the samples with the diamond lapping from 30 μm to 0.02 μm. For the final lapping (0.02 μm), there will

be no changes in friction. A standard 10-minute polishing is needed for this lapping paper. The procedure of polishing is shown in figure 29.

4.5.1.3 Polymer solutions: spin-coater

Model WS-650MZ-23NPPB 0 spin-coater is purchased from Laurell Technologies Corporation, which spin coats thin film samples for FDTR measurements.

The dissolvable polymer can be spin-coated to make standard FDTR samples. First, polymers are dissolved in volatile solutions like toluene under a relatively high dilution ratio (1%-10%). The concentration of the polymer is dependent on the parameters of the spin-coater. Then, set a pre-determined spin speed and time. Fix a glass substrate onto the spin-coater with vacuum suction, then put several polymer solution droplets onto the glass substrate until the glass surface is fully covered with liquid. Then, start the coating and do not move out the sample until the coater is stopped.

4.5.2 Transducer layer deposition

Transducer layer deposition is finished with CVC SC4500 Combination Thermal/ E-gun Evaporation System (SC4500 Odd-Hour Evaporator) in CNF.

4.5.2.1 Gold layer deposition

The transducer layer will convert the laser energy into heat around the laser landing spot. Most importantly, the metal transducer has temperature dependence on its reflectivity, making it eligible for a temperature transducer even though there are reports about conducting FDTR measurement without a metal transducer layer. However, their work is mainly limited to certain kinds of samples.[16]

For transducer layer deposition, first place the samples in the vacuum chamber. The vacuum pump will decrease the pressure to under 2×10^{-6} Torr. Then an e-gun will bombard the gold source to heat the gold gradually. When the gold is hot enough, it will evaporate and

homogeneously grow onto the sample surface. A shutter will terminate the deposition when the gold layer reaches desired thickness. The tooling factor for gold layer deposition is 80%, and the deposition speed is 1 angstrom/s. After the deposition, cool down the system before pumping in air to reach atmospheric pressure.

4.5.2.2 Titanium adhesion layer deposition

The vacuum step is identical to the gold layer deposition. Heat the titanium source with an e-gun and do a 5 nm layer adhesion layer deposition. The tooling factor for the titanium adhesion layer is 80%, and the deposition speed is 0.1 angstrom/s. After the titanium adhesion layer deposition is the gold layer deposition, switch the titanium source to gold source after thoroughly cooled. The gold deposition step is identical to the previous step.

4.5.3 Sample characterization

4.5.3.1 Thickness measurements

Any deposited sample should be measured with a profilometer to ensure the deposition quality (surface roughness) and deposition layer thickness. P7 and P10 profilometer have the same operation procedure and the same accuracy. Take the P7 profilometer for an example, the tip force is set to be 1 mg, and the scanning speed is 50 $\mu m/s$. A left-to-right scanning (or right-to-left) can confirm the surface topology of the sample. The sample thickness can be derived from the height difference between the sample and the substrate under it.

4.5.3.2 Other information

XRR (x-ray reflectivity) can determine the sample's density, thickness, and composition for other layer information. An optical microscope can roughly determine the surface topology of the sample.

4.6 Measurement Results

Au-Ti-Silica (gold-coated silica sample with titanium adhesion layer) is used as our reference sample. A typical measurement for such a sample is shown in figure 30. The fitted value for the Au-Ti-Silica reference sample is 1.40.

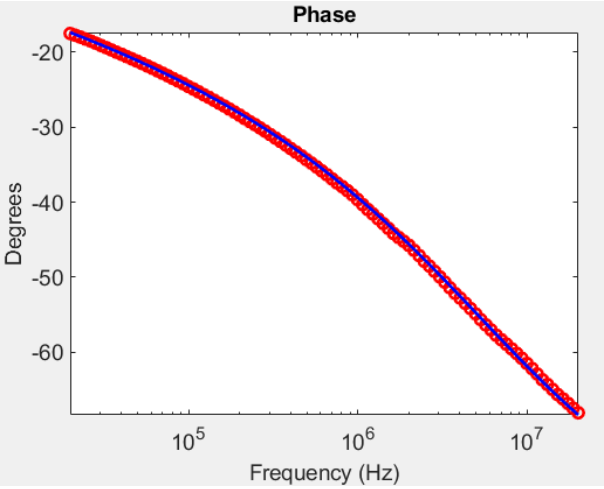

Figure 30: Matlab fitting for Au-Ti-Silica reference sample

References

[1] Abad, B., Borca-Tasciuc, D. A. & Martin-Gonzalez, M. S. Non-contact methods for thermal properties measurement. *Renew. Sustain. Energy Rev.* **76**, 1348–1370 (2017).

[2] Wang, T. *et al.* Rapid and high precision measurement of opto-thermal relaxation with pump-probe method. *Sci. Bull.* **63**, 287–292 (2018).

[3] Grumstrup, E. M., Gabriel, M. M., Cating, E. E. M., Van Goethem, E. M. & Papanikolas, J. M. Pump-probe microscopy: Visualization and spectroscopy of ultrafast dynamics at the nanoscale. *Chem. Phys.* **458**, 30–40 (2015).

[4] He, W., Yurkevich, I. V., Zakar, A. & Kaplan, A. High-frequency conductivity of optically excited charge carriers in hydrogenated nanocrystalline silicon investigated by spectroscopic femtosecond pump-probe reflectivity measurements. *Thin Solid Films* **592**, 287–291 (2015).

[5] Xian, Y., Zhang, P., Zhai, S., Yuan, P. & Yang, D. Experimental characterization methods for thermal contact resistance: A review. *Appl. Therm. Eng.* **130**, 1530–1548 (2018).

[6] Zhu, J., Tang, D., Yang, R., Liu, J. & Wang, W. Frequency-domain Thermoreflectance technique for measuring thermal conductivity and interface thermal conductance of thin films. *Int. Heat Transf. Conf.* 1–9 (2014).

[7] Goni, M., Patelka, M., Ikeda, S., Sato, T. & Schmidt, A. J. Frequency domain thermoreflectance technique for measuring the thermal conductivity of individual micro-particles. *Rev. Sci. Instrum.* **89**, (2018).

[8] Schmidt, A. J. Optical characterization of thermal transport from the nanoscale to the macroscale. (MIT, 2008)

[9] Schmidt, A. J., Cheaito, R. & Chiesa, M. A frequency-domain thermoreflectance method for the characterization of thermal properties. *Rev. Sci. Instrum.* **80**, (2009).

[10] Schmidt, A., Chiesa, M., Chen, X. & Chen, G. An optical pump-probe technique for measuring the thermal conductivity of liquids. *Rev. Sci. Instrum.* **79**, (2008).

[11] Yang, J., Maragliano, C. & Schmidt, A. J. Thermal property microscopy with frequency domain thermoreflectance. *Rev. Sci. Instrum.* **84**, (2013).

[12] Yang, J. Thermal property measurement with frequency domain Thermoreflectance. (Boston University, 2016)

[13] Regner, K. T., Majumdar, S. & Malen, J. A. Instrumentation of broadband frequency domain thermoreflectance for measuring thermal conductivity accumulation functions. *Rev. Sci. Instrum.* **84**, (2013).

[14] Regner, K. T. *et al.* Broadband phonon mean free path contributions to thermal conductivity measured using frequency domain thermoreflectance. *Nat. Commun.* **4**, 1640–1647 (2013).

[15] Adhesives and Mountants for Materials Science & Metrology. https://www.emsdiasum.com/microscopy/products/materials/adhesives.aspx#50400.

[16] Wang, L., Cheaito, R., Braun, J. L., Giri, A. & Hopkins, P. E. Thermal conductivity measurements of non-metals via combined time- and frequency-domain thermoreflectance without a metal film transducer. *Rev. Sci. Instrum.* **87**, (2016).

5 Challenges

In this thesis, the challenges are mainly from FDTR systems, while for LFA, it is mainly instrumental limitations that prevent us from getting measurements on more complicated samples.

For LFA measurements, there is some inconsistency in the measurements. There is a slight fluctuation in the sample temperature, where there will be a temperature increase in the oven after a while. The temperature sensor of LFA is not sensitive enough to combat these fluctuations. Also, when fitting with XFALT software, the software cannot automatically find the optimal measurement time. Manual fine-tuning of the measurement time is crucial for obtaining accurate thermal diffusivity values.

For FDTR, even though it opens a bunch of opportunities for thermal measurements. There are, however, more challenges. First, laser power is essential in each measurement. If the laser power is too weak, there will be a large noise-to-signal ratio, making the measurement not accurate enough. For samples like organic polymers or crystals, too strong a laser power will only lead to rapid degradation of the sample. It is hard to balance between different laser powers. Second, FDTR has some harsh requirements for sample pretreatment. Both transducer layer deposition and surface polishing are required for most samples. Also, we need to obtain many other related parameters to get a fitted result, where many of these parameters (like heat capacity, thermal conductivity, and thickness) are challenging to get. Third, for alignment, our system is entirely manual. After some time of use (usually about two weeks), we need to manually adjust the system to perfect the alignment, which can take much time.

6 Conclusion

Thermal measurements of samples with different layer structures are of great significance in both industrial and academic areas. Obtaining precise thermal properties makes it possible to fabricate complicated systems with controllable thermal management. However, as new materials keep emerging, enormous challenges are posed on conventional thermal measurements. For modern thermal measurements, convenience, accuracy, and sample requirements are becoming the three most important factors. This thesis addressed how to measure different samples and set up an FDTR system for advanced thermal measurements.

Laser flash is a most promising technique for measuring bulk, single-structured samples. In this thesis, we showed LFA measurements on BN/silicone composites and silicone/Glycerol composites. LFA can rapidly analyze a large number of samples with high precision and giving their thermal diffusivities. After heat capacity measurements with DSC, the corresponding thermal conductivity can be obtained. The advantages of using the LFA technique are its convenience and relatively low cost. However, LFA also has many major drawbacks. It can only measure bulk samples with flat surfaces; it can only measure single component materials, and it can only give one thermal parameter – thermal diffusivity.

FDTR

FDTR system solves almost all the issues from LFA measurements. Using lasers as its probes can measure almost all kinds of samples, as long as their surface is smooth enough to reflect the lasers. This thesis demonstrated how to set up an FDTR system properly and showed how to do the beam/optics alignment step by step. Details of sample preparation and parameter measurements are also discussed in this thesis. FDTR system can give detailed data of multiple parameters. We can measure volumetric heat capacity, thermal conductivity, interfacial conductance, anisotropic ratio, and thickness of the sample in our setup.

Moreover, when paired with other equipment, there is much more potential in the FDTR system. For example, when paring the FDTR system with a piezo stage controlled with a computer, it is possible to give a 2D thermal conductivity mapping of the samples. Overall, FDTR opens up a door for intricate material systems with controllable thermal properties and will keep shining its importance in thermal measurements as more implements are added.